SEGMENTATION UNDER OCCLUSIONS USING SELECTIVE SHAPE PRIOR*

SHESHADRI. R. THIRUVENKADAM†, TONY. F. CHAN ‡, AND BYUNG-WOO HONG§

Abstract. In this work, we address the problem of segmenting multiple objects, under possible occlusions, in a level set framework. A variational energy that incorporates a piecewise constant representation of the image in terms of the object regions and the object spatial order is proposed. To resolve occluded boundaries, prior knowledge of shape of objects is also introduced within the segmentation energy. By minimizing the above energy, we solve the *segmentation with depth* problem, i.e. estimating the object boundaries, the object intensities, and the spatial order. The segmentation with depth problem was originally dealt with by the *Nitzberg-Mumford-Shiota* (NMS) variational formulation which proposes segmentation energies for each spatial order. We discuss the relationships, and show the computational advantages of our formulation over the NMS model, mainly due to our treatment of spatial order estimation within a *single* energy. A novelty here is that the spatial order information available in the image model is used to dynamically impose prior shape constraints *only* to occluded boundaries. Also presented are experiments on synthetic and real images with promising results.

Key words. image segmentation, variational methods, level set methods

1. Introduction. Image segmentation is an important step in understanding the composition of the original 3D scene that gave rise to the image. However, it is often considered a difficult problem due to noise which results in spurious edges and boundary gaps, and occlusions which leads to a overlap of object boundaries. Low-level visual features such as intensity, color and texture are generally not sufficient to overcome such difficulties that would make purely bottom-up segmentation approaches unsuccessful. This naturally leads to a need for integrating low-level features and high-level information in segmentation. Enforcing a prior knowledge on the shape of objects is a common way to facilitate segmentation especially under low contrasts, occlusions and other undesirable noisy conditions.

In this paper, we address the problem of segmenting multiple objects with possible occlusions, and recover the object spatial order whenever possible. Here, a segmentation energy incorporating shape prior knowledge is presented in a variational framework. The novelty here is that we identify the spatial order to be encoded within a piecewise constant representation of the given image, and hence are able to recover the spatial order as part of the segmentation process. We demonstrate how the above spatial order information can be used within the energy to impose the shape prior only to occluded boundaries.

Our model solves the *segmentation with depth* problem that aims to determine the boundaries of overlapping objects, along with their spatial ordering, based on intensity distributions in the object regions. The segmentation with depth problem has been addressed before in a variational framework by Nitzberg, Mumford and Shiota (NMS) in [28, 29] and numerical methods for minimizing the NMS model have been presented in [16, 36]. In the NMS approach, for each spatial order of the objects, a segmentation energy is minimized using curvature continuity to complete occluded

*A preliminary version of this work appears in the conference proceedings of SSVM'07. This research is supported by ONR grant N00014-06-1-0345, and NSF grant DMS-0610079.

†Department of Mathematics, University of California, Los Angeles, sheshad@math.ucla.edu.

‡Professor of Mathematics, University of California Los Angeles, and Assistant Director, Directorate for Mathematics & Physical Sciences, The National Science Foundation, chan@math.ucla.edu.

§Computer Science Department, University of California, Los Angeles, hong@cs.ucla.edu.

boundaries. Then the smallest of the above energy-minima would give the spatial order of the objects along with their boundaries and intensities. In contrast, our formulation involves only *one* segmentation energy with the spatial order given by the estimation of a sequence of constants. Thus the main computational expense in the NMS approach which is of the order of $N.N!$ shape optimizations (for N objects in the scene) is reduced to just N shape optimizations in our case. We will provide a detailed comparison of our model with the NMS approach in the following sections.

In our work, the contours that segment the object-boundaries are represented using the *level set method* [14, 15, 30], and are evolved by gradient descent of our variational energy. Deformable models, often called *Snakes*, initially proposed by Kaas et al. [19] evolve an explicitly parametrized contour based on external and internal energies. Despite wide use and popularity due to its simplicity and speed, the Snakes approach has the drawbacks of being dependent on the initial contour placement, and is restricted by the topology of the contour. There have been some works to overcome these limitations [2, 10, 17, 1, 24, 13].

In the level set framework, the contour is represented implicitly as the zero level of a higher dimensional embedding function, and the contour propagation is performed by evolving the embedding function. This enables one to handle topological changes of the boundary such as splitting and merging easily. Segmentation algorithms using the level set method have been developed based on the geometric heat equation taking into account the strength of the edgeness by Caselles et al. [3], Chopp [9], and Malladi et al. [23]. The modified edge-based energy formulations of the above equation termed *geodesic active contours* have been proposed by Caselles et al. [4] and by Kichenassamy et al. [20, 21]. However, these approaches based on local image gradient features are still highly sensitive with respect to the initial contour placement. In order to overcome this undesired behavior, region-based energy formulations have been introduced in [26, 37, 6, 34, 31].

Most of the region-based approaches are based on the popular *Mumford-Shah functional* [26, 27] which finds a piecewise smooth representation for a given noisy image. A level-sets based active-contour implementation of the piecewise constant, two-phase version of the Mumford-Shah functional has been developed by Chan and Vese (CV) [6]. Their use of region-based information within an implicit framework gave the advantages of segmenting objects of unknown topology, robustness to noise, dis-continuous edges and contour initialization, and detection of interior of objects. The CV model has also been extended to allow the segmentation of multiple disjoint objects/phases using a multiphase level set formulation [35]. Our segmentation model is similar to some of the above region based approaches in seeking for a piecewise constant representation of the given image. But in addition to this representation, we also want to recover the actual object boundaries (possibly occluded) along with their spatial order (whenever well-defined).

The above segmentation methods solely rely on image intensity which is not sufficient to detect missing edges that could occur due to occlusions/low-contrast often observed in many practical applications. This consequently leads to the efforts that introduce prior shape information into segmentation schemes [18]. Chen et al. [7, 8] propose a level set segmentation algorithm based on geodesic active contours, incorporating an explicit registration term measuring shape similarity between the segmenting curve and a prior shape that is modeled by the distance function. The active shape model [11] using principal component analysis from a set of training shapes has been used as prior shape information. The level set segmentation algorithm incorporating

statistical shape priors has been proposed in [34, 33, 22, 25] where principal component analysis is performed based on a set of training shapes in the form of signed distance functions. In contrast to a conventional linear PCA, a nonlinear statistics by means of kernel PCA is considered as a shape model in [12]. In most works, a rigid transformation is considered in the comparison of the shape between the evolving level set function and the shape prior model, but a projective transformation is considered by slicing the signed distance function at various angles in [32]. A region-based level set segmentation algorithm with shape priors has been proposed by Chan et al [5].

Although incorporating a shape prior within our segmentation model was inspired by the above works, our method has a novelty in that, the use of shape prior knowledge is automatically restricted *only* to occluded parts of the object boundaries. That is, the algorithm selectively activates the shape term within the energy functional *only* for occluded regions. Thus, the evolution of the segmenting level set function for the unoccluded regions is solely driven by image intensity, even though the governing energy functional also includes the shape term. This selective use of local prior shape avoids enforcing shape constraints on regions where the object boundary is clearly defined by image intensity.

The focus of this paper is to solve the segmentation from depth problem using prior knowledge of shape of objects. Using the spatial order information, we demonstrate one possible application where the shape constraints are activated only for occluded boundaries. The question on the kind of shape prior knowledge to be used depends on the application, and is not dealt with here. In this work, for convenience, we deal with object boundaries that can be characterized by an *explicit prior-shape* (given by a binary image). While assuming the availability of such a prior knowledge may seem restrictive, its use has been demonstrated before by many shape-based segmentation methods, especially for medical imaging applications.

To summarize, we first present a piecewise constant image representation of an occlusion scene, in terms of the object regions and their intersection regions. We then identify from the above representation that the sequence of constants corresponding to the intersection regions is unique to the object spatial order. The inverse problem is given by a constrained energy minimization that estimates the object boundaries, intensities, and the sequence of constants which determines the spatial order. We show that this constrained minimization is identical to the NMS minimization, but is computationally less expensive. Also, in our experiments, we approximate the above problem as an unconstrained energy minimization and have obtained identical results for images corrupted with white noise. A key contribution here is that the spatial order information available through the sequence of constants can be used within the energy to dynamically impose the shape prior only to occluded boundaries.

2. Nitzberg-Mumford-Shiota formulation. We will briefly review the related formulation of NMS [29] for segmentation with depth. In a later section, we will present detailed comparisons with our approach. We start with some basic definitions and assumptions. Suppose that $I : \Omega \to \mathbb{R}$, $\Omega \subset \mathbb{R}^2$ is a 2D image of a scene composed of N objects $\{O_p\}_{p=1}^N$. We define an *occlusion* relation '$>$' on object indices given by $i > j$ when O_i is in front of O_j (from the viewer's perspective). We denote a *spatial order* of the objects by the ordered set of object indices $Q^k = \{i_1 > i_2 > .. > i_N\}$, and by $\mathbf{Q} = \{Q^1, Q^2, ..., Q^{N!}\}$ the set of $N!$ possible spatial orders. Let $\{A_p\}_{p=1}^N$ be the regions formed on the image domain by the objects. Now suppose that we have the following assumptions:

- The image intensity formed by the objects O_k is close to a constant c_k, and the background intensity is close to a constant, $\tilde{c}$.
- The objects are not twisted between themselves.

Due to the assumptions listed above, for a spatial order $\{i_1 > i_2 > .. > i_N\}$, $A_k - \cup_{j>k} A_j$ is the visible portion of the object O_k, with image intensity close to a constant c_k. For the topmost object, O_{i_1}, let $\cup_{j>i_1} A_j = \{\phi\}$. Thus for a given spatial order Q^k, the image I of the scene can be represented in terms of the visible object regions,

$$I = \sum_{q=1}^{N} c_q \chi_{A_q - \cup_{j>q} A_j} + \tilde{c} \prod_{q=1}^{N} (1 - \chi_{A_k}) \tag{2.1}$$

where χ_S is the characteristic function of a set S.

2.1. NMS minimization. Given an image I_0, for each spatial ordering Q^k of objects, $(k = 1, 2, .., N!)$, the NMS segmentation-energy for Q^k is written with respect to object regions A_p, constant intensities c_p and background intensity $\tilde{c}$. Denote $\mathbf{A} = \{A_1, A_2, .., A_N\}$, $C_{obj} = \{c_1, c_2, ..c_N, \tilde{c}\}$,

$$\tilde{E}_{Q^k}[\mathbf{A}, C_{obj}] = \sum_{p=1}^{N} \int_{A_p - \cup_{j>p} A_j} (I_0 - c_p)^2 dx + \int_{\cap_{k=1}^{N} A_k^c} (I_0 - \tilde{c})^2 dx$$
$$+ \sum_{p=1}^{N} \lambda \int_{\partial A_p} ds + \beta \int_{\Omega} \hat{S}(A_p) dx \tag{2.2}$$

Here, the fourth term is the prior knowledge that the NMS model incorporates to resolve occlusions. Specifically in their work, $\hat{S}$ is used to complete occluded boundaries by continuity of curvature, and is given by

$$\hat{S}(A_p) = \phi(\kappa_p),$$

where the function $\phi(x)$ is to be a positive, convex, even function. κ_p is the curvature of ∂A_p. Our model also uses a prior shape term to resolve occlusions, although for a different choice of $\hat{S}$.

The NMS model is the following minimization problem

$$\min_{k \in \{1,2,..,N!\}} \min_{\mathbf{A}, C_{obj}} \tilde{E}_{Q^k} \tag{2.3}$$

A minimizer m determines the spatial ordering Q^m, the object regions $\mathbf{A}^m$, and the intensities C^m_{obj}.

3. Occlusion Model. In the NMS model (2.3), the spatial order estimation is done via $N!$ segmentation-energy minimizations, and turns out to be computationally expensive in spite of a close initial guess for the object regions. The reason is that the spatial order is not characterized within the image model (2.1) and hence cannot be "adapted" based on the object regions.

To deal with the issue of spatial order estimation, we want to first look at an image representation that is *rich* enough to hold information on the object regions, object intensities, and the spatial order. In the following discussion, we observe a dependence between intensities in the intersection regions and the spatial order. Later, we utilize this dependence to incorporate spatial order within a *single* segmentation-energy.

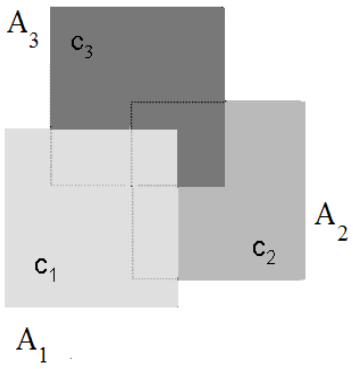

FIG. 3.1. *Image formed for 3 objects, A_k with constant intensity c_k, for spatial order $1 > 3 > 2$. The dotted lines are the occluded boundaries of A_2 and A_3.*

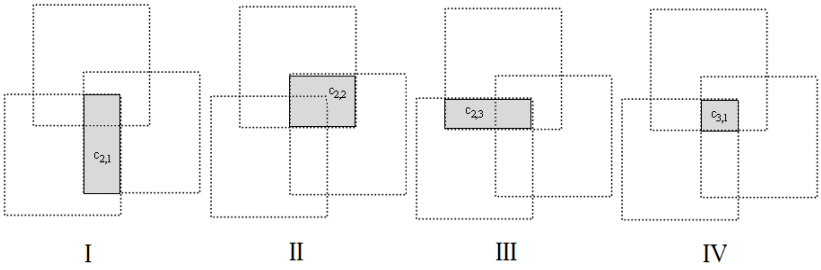

FIG. 3.2. *Intersection regions $P_{p,k}$ (gray colored) and corresponding constants $c_{p,k}$. (I) $P_{2,1}$ (II) $P_{2,2}$ (III) $P_{2,3}$ (IV) $P_{3,1}$. For spatial order $1 > 3 > 2$ as in Fig. 3.1, $\big(c_{2,1} = c_2,\ c_{2,2} = c_2,\ c_{2,3} = c_3,\ c_{3,1} = c_2\big)$.*

To motivate the form of the image I, in the case $N = 3$, suppose that (WLOG) $1 > 3 > 2$ is the spatial order of the objects, A_1, $A_3 - A_1$ and $A_2 - (A_1 \cup A_3)$ are the parts of the objects O_1, O_3 and O_2 visible in the image (Fig. 3.1). Thus we have from (2.1),

$$\begin{aligned} I &= c_1\chi_{A_1} + c_2\chi_{A_3 - A_1} + c_3\chi_{A_2-(A_1\cup A_3)} + \tilde{c}(1-\chi_{A_1})(1-\chi_{A_2})(1-\chi_{A_3}) \\ &= c_1\chi_{A_1} + c_2\chi_{A_2} + c_3\chi_{A_3} - c_2\chi_{A_1\cap A_2} - c_2\chi_{A_2\cap A_3} - c_3\chi_{A_1\cap A_3} + c_2\chi_{A_1\cap A_2\cap A_3} \\ &\qquad + \tilde{c}(1-\chi_{A_1})(1-\chi_{A_2})(1-\chi_{A_3}) \end{aligned} \tag{3.1}$$

In the above expression, for each intersection region, the corresponding constant factor equals the intensity of the farthest object in that intersection. Hence the spatial order is *encoded* within the sequence of intersection-constants $\{c_2, c_2, c_3, c_2\}$.

For the general case of N objects with a spatial order $i_1 > i_2 > .. > i_N$, the image I of the scene in terms of the visible object-regions is given by

$$I = \sum_{k=1}^{N} c_k \chi_{A_k - \cup_{j>k} A_j} + \tilde{c} \prod_{k=1}^{N} (1 - \chi_{A_k})$$

Similar to (3.1), rewriting the above expression in terms of the regions A_k and their

TABLE 3.1

$N = 3$ case: Constants $c_{p,k}$ corresponding to intersection regions $P_{2,1} = A_1 \cap A_2$, $P_{2,2} = A_1 \cap A_3$, $P_{2,3} = A_2 \cap A_3$, $P_{3,1} = A_1 \cap A_2 \cap A_3$

Spatial Order Q^k	$S^k = \{c_{2,1}, c_{2,2}, c_{2,3}, c_{3,1}\}$
$1 > 2 > 3$	$\{c_2, c_3, c_3, c_3\}$
$1 > 3 > 2$	$\{c_2, c_2, c_3, c_2\}$
$2 > 1 > 3$	$\{c_1, c_3, c_3, c_3\}$
$2 > 3 > 1$	$\{c_1, c_1, c_3, c_1\}$
$3 > 2 > 1$	$\{c_1, c_1, c_2, c_1\}$
$3 > 1 > 2$	$\{c_2, c_1, c_2, c_2\}$

intersection regions, gives the following general form of I, valid for *any* spatial ordering between the objects,

$$I = \sum_{p=1}^{N} c_p \chi_{A_p} + \sum_{p=2}^{N} \sum_{k=1}^{\binom{N}{p}} (-1)^p c_{p,k} \chi_{P_{p,k}} + \tilde{c} \prod_{k=1}^{N} (1 - \chi_{A_k}) \tag{3.2}$$

Here, $P_{p,k}$, $(p = 2, 3..N, k = 1, 2, ..\binom{N}{p})$ is the k^{th} unordered *intersection* of, p *regions* from $A_1, A_2, ..., A_N$. $c_{p,k}$ are positive constants and take one of the values $c_1, c_2, ...c_N$. In fact, $c_{p,k}$ takes the intensity of the farthest object appearing in the intersection, $P_{p,k}$. For $N = 3$, the regions $P_{p,k}$ and the constants $c_{p,k}$ are shown in Fig. 3.2.

Thus, there are $N!$ possible sequences for $c_{p,k}$, with each sequence corresponding to a unique spatial ordering of the objects. For $i = 1, 2, .., N!$, let S^i denote the sequence of constants $c_{p,k}$, corresponding to the spatial ordering of the objects, Q^i. We denote $\mathbf{S} = \{S^1, S^2, ..., S^{N!}\}$, the set of *spatial order sequences* corresponding to the set of spatial orders $\mathbf{Q} = \{Q^1, Q^2, ..., Q^{N!}\}$.

For the $N = 2$ case,

$$I = c_1 \chi_{A_1} + c_2 \chi_{A_2} - c_{2,1} \chi_{A_1 \cap A_2} + \tilde{c}(1 - \chi_{A_1})(1 - \chi_{A_2}).$$

Here, $c_{2,1} = c_2$ iff $1 > 2$, and $c_{2,1} = c_1$ iff $2 > 1$.

Similarly for $N = 3$,

$$I = c_1 \chi_{A_1} + c_2 \chi_{A_2} + c_3 \chi_{A_3} - c_{2,1} \chi_{A_1 \cap A_2} - c_{2,2} \chi_{A_2 \cap A_3} - c_{2,3} \chi_{A_1 \cap A_3} + c_{3,1} \chi_{A_1 \cap A_2 \cap A_3} + \tilde{c}(1 - \chi_{A_1})(1 - \chi_{A_2})(1 - \chi_{A_3}),$$

and Table 3.1 shows the values $c_{p,k}$ for possible occlusion scenario.

4. Energy formulation. As seen above, (3.2) gives a piecewise constant representation of the image in terms of the objects in the scene, along with their spatial order. Given an image I_0, we solve the inverse problem of recovering the object regions $\{A_p\}_{p=1}^{N}$, the object intensities $c_1, c_2, ..c_N$, the background intensity $\tilde{c}$, and the intersection intensities $c_{p,k}$. Denote $\mathbf{A} = \{A_1, A_2, .., A_N\}$, $C_{obj} = \{c_1, c_2, ..c_N, \tilde{c}\}$, and sequence $C_{int} = \{c_{p,k} |\ p = 2, 3..N,\ k = 1, 2, ..\binom{N}{p}\}$. The sequence C_{int} is constrained to adhere to one of the $N!$ possible spatial order sequences S^i. We formulate the above problem as the following energy minimization. Here, a *prior shape* term is introduced

within the energy to resolve occluded object boundaries.

$$E[\mathbf{A}, C_{obj}, C_{int}] = \int_\Omega \big(I_0 - (\sum_{p=1}^{N} c_p \chi_{A_p} + \sum_{p=2}^{N}\sum_{k=1}^{\binom{N}{p}} (-1)^p c_{p,k}\chi_{P_{p,k}} + \tilde{c}\prod_{k=1}^{N}(1-\chi_{A_k}))\big)^2 dx + \sum_{p=1}^{N}\big(\lambda\int_{\partial A_p} ds + \beta\int_\Omega \hat{S}(A_p)dx\big)$$

$$\text{s.t, } C_{int} \in \mathbf{S} = \{S^1, S^2, ..., S^{N!}\}. \tag{4.1}$$

We note that the above energy is quadratic with respect to the constants C_{obj} and C_{int}. Since the sequence of constants S^k corresponds to spatial order Q^k, a minimizing C_{int}^{min} for the energy would determine a spatial order for the objects. Whether a unique solution C_{int}^{min} exists or not would depend on the number of non-empty intersection regions between objects $\mathbf{A}$. However, as in many cases to be discussed in Section 7, even partial information of elements of the sequence C_{int}^{min} is sufficient to give a unique projection onto the set $\mathbf{S}$ (thus solving the segmentation with depth problem). For example, we see from Table 3.1 that just estimating the first two elements of C_{int}, $c_{2,1} = c_2$ and $c_{2,2} = c_3$ would determine the spatial order as $1 > 2 > 3$.

The second term is a length regularization term, commonly used in shape optimization problems, and the third term constrains the shape of the boundaries of A_p. There are various choices for the shape term such as the Euler's elastica energy (to enforce curvature continuity of A_p), statistical/explicit shape priors depending on the kind of application. In this work, we mainly consider the application of shape explicitly, with the term $\int_\Omega \hat{S}(A_p)$ measuring the area dissimilarity of the object A_p from a given binary shape S. λ and β are parameters that balance the terms. Later, in Section 8, we also show how one can selectively impose shape constraints, only to occluded object boundaries.

In our work, for computational simplicity, we have assumed the constants $c_{p,k}$ to be independent, and minimize (4.1) without constraints

$$\min_{\mathbf{A}, C_{obj}, C_{int}} E \tag{4.2}$$

Then, the minimizing constants C_{int}^m can be post-processed to deduce a unique spatial order for images with unambiguous occlusions. Our experiments indicate that, for images with uncorrelated noise, the above simplified approach (4.2) takes solutions very close to that of the original constrained minimization problem (4.1).

5. Related Works. The form of (4.1) indicates its relationship to some of the region-based segmentation approaches e.g. [35]. Without the constraint on C_{int} and for $\beta = 0$, (4.1) is just the *cartoon* Mumford-Shah functional that seeks a piecewise constant approximation to a given I_0. But this is not sufficient to recover object boundaries that are occluded. For a non-zero β, one can also recover occluded boundaries due to the shape term, and the estimated C_{int} in many cases defines a unique spatial order. The constraint on C_{int} gives the model additional robustness to the segmentation of non-white noise images. However as observed in Section 11, the minimizers obtained for white noise images do not depend on the constraint.

5.1. Comparisons with the NMS model. Here, we compare our energy (4.1) with the NMS model (2.3). The NMS segmentation-energy for a spatial order Q^k, (2.2), is given by

$$\tilde{E}_{Q^k}[\mathbf{A}, C_{obj}] = \sum_{p=1}^{N} \int_{A_p - \cup_{j>p} A_j} (I_0 - c_p)^2 dx + \int_{\cap_{k=1}^{N} A_k^c} (I_0 - \tilde{c})^2 dx + \sum_{p=1}^{N} \lambda \int_{\partial A_p} ds + \beta \int_{\Omega} \hat{S}(A_p) dx$$

The first term of the above energy is rewritten as follows

$$\sum_{p=1}^{N} \int_{A_p - \cup_{j>p} A_j} (I_0 - c_p)^2 dx = \int_{\Omega} (I_0 - \sum_{p=1}^{N} c_p \chi_{A_p - \cup_{j>p} A_j})^2 dx$$
$$= \int_{\Omega} (I_0 - (\sum_{p=1}^{N} c_p \chi_{A_p} + \sum_{p=2}^{N} \sum_{k=1}^{\binom{N}{p}} (-1)^p c_{p,k} \chi_{P_{p,k}}))^2 dx$$

where the above sequence $C_{int} = \{c_{p,k} |\ p = 2, 3..N,\ k = 1, 2, ..\binom{N}{p}\} = S^k$, corresponds to the spatial order Q^k. Thus we have

$$\tilde{E}_{Q^k}[\mathbf{A}, C_{obj}] = E[\mathbf{A}, C_{obj}, C_{int} = S^k].$$

It follows that

$$\min_{k \in \{1,2,...N!\}} \min_{\mathbf{A}, C_{obj}} \tilde{E}_{Q^k} = \min_{k \in \{1,2,...N!\}} \min_{\mathbf{A}, C_{obj}, C_{int} = S^k} E$$
$$= \min_{\mathbf{A}, C_{obj}, C_{int} \in \{S^1, S^2, ..., S^{N!}\}} E$$

Hence the NMS model (2.3) and the minimization of (4.1) are equivalent. The key contribution here is that we have written the $N!$ minimizations of energies $\tilde{E}_{Q^k}[\mathbf{A}, C_{obj}]$ as a *single* energy minimization of $E[\mathbf{A}, C_{obj}, C_{int} \in \{S^1, S^2, ..., S^{N!}\}]$ by introducing additional variables C_{int} to estimate the spatial ordering of the objects. The main computational expense in both models (4.1) and (2.2) is the minimization with respect to regions $\mathbf{A}$. The (NMS) model is more expensive because of the $N.N!$ shape minimizations it has to deal with, in contrast to just N shape minimizations in our case. Further, in the (NMS) model, in spite of a close initial guess for object boundaries, one has to go through each of the $N!$ minimizations in order to find the correct spatial order. Whereas in our energy, which is quadratic with respect to the variable C_{int}, allows one to utilize projection-gradient type algorithms for fast convergence to the correct spatial order even for rough initial guesses for object boundaries. The problem is further simplified for white noise images when the unconstrained energy (4.2) can be used, and the estimated C_{int} can be post-processed to infer the spatial order.

We will further illustrate the above differences through examples in the experiments section. In the subsequent sections, we discuss the implementation details and experimental results for the unconstrained energy (4.2).

6. Level Set Formulation. The regions A_k are represented as the interior of level set functions ϕ_k, i.e. $H(\phi_k) = \chi_{A_k}$, $k = 1, 2, ..., N$, where $H(t)$ is the Heaviside function. Thus, we try to recover ϕ_k from I_0. Let $\Phi = (\phi_1, \phi_2, .., \phi_N)$, and as before $C_{obj} = \{c_1, c_2, ..c_N, \tilde{c}\}$, and sequence $C_{int} = \{c_{p,k} |\ p = 2, 3..N,\ k = 1, 2, ..\binom{N}{p}\}$. We reformulate the problem (4.2) as the minimization with respect to Φ and C_{obj}, C_{int}, of following energy:

$$E[\Phi, C_{obj}, C_{int}] = \int_\Omega \big(I_0 - \sum_{p=1}^{N}\sum_{k=1}^{\binom{N}{p}}(-1)^{p-1}c_{p,k}S_{p,k} - \tilde{c}\tilde{S}_b\big)^2 dx + \lambda\int_\Omega \sum_{k=1}^{N}|\nabla H(\phi_k)| + \beta\int_\Omega \sum_{k=1}^{N}\hat{S}(\phi_k)dx \quad (6.1)$$

where, $S_{p,k}$ is k^{th} unordered product of p functions from $H(\phi_1), H(\phi_2), ..., H(\phi_N)$ and $\tilde{S}_b = \prod_{k=1}^{N}(1 - H(\phi_k))$. The second term regularizes Φ, and the last term constrains the shape of the 0-levelset of ϕ_k. λ and β balance the three terms.

For simplicity, we will illustrate the $N = 2$ case. The above energy reduces to:
$E[\phi_1, \phi_2, c_1, c_2, c_{2,1}, \tilde{c}] =$

$$\int_\Omega \big(I_0 - (c_1H(\phi_1) + c_2H(\phi_2) - c_{2,1}H(\phi_1)H(\phi_2) + \tilde{c}(1 - H(\phi_1))(1 - H(\phi_2)))\big)^2 dx + \lambda\big(\int_\Omega |\nabla H(\phi_1) + \int_\Omega |\nabla H(\phi_2)|\big) + \beta\int_\Omega \hat{S}(\phi_1) + \hat{S}(\phi_2)dx \quad (6.2)$$

The fourth term is used to impose shape-based constraints such as curvature, and explicit shape on the objects $H(\phi_i)$. This term is used to avoid local minima of the first term in (6.2) that occur particularly under occlusions. In our implementation, we only deal with imposing constraints on length (to resolve linear edges that are occluded) and explicit shape (given by a binary image).

Note: In (6.1), the N level set functions are used to partition Ω into 2^N piecewise constant, disjoint regions, i.e. N visible regions of the objects, $2^N - N - 1$ occlusion regions, and the background. Here N level set functions are used for N objects to allow for the maximum possible number of $2^N - N - 1$ occlusions between the objects. In fact to represent an occlusion scenario of N objects with M occlusions ($M \leq 2^N - N - 1$), and the background, we need an optimal number of $\log_2(N + M + 1)$ level set functions. For instance, the multi-phase version of the CV model assumes the objects/phases to be disjoint, and hence needs only $\log_2 N$ (the background is also treated as an object) level set functions to partition Ω.

7. Spatial Order Estimation. Once (6.1) is minimized, the solutions C_{int}^{min} and C_{obj}^{min} are compared to infer the spatial order. To start with, we consider non-empty intersection regions to infer the occlusion relation '>' for possible object pairs. Then, for certain classes of images without occlusion ambiguities and with sufficient number of non-empty object intersections, the occlusion relation determines the spatial order.

7.1. Dis-Occluding intersection regions. First, the mean intensities in non-empty intersection regions are compared with the object intensities, to infer the object

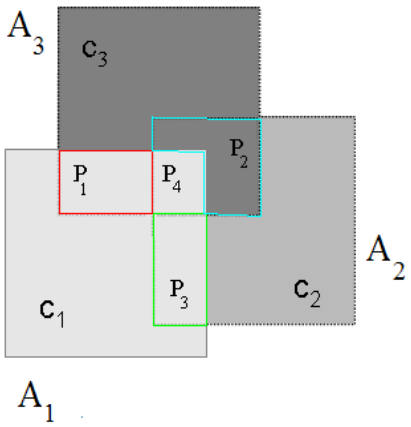

FIG. 7.1. *Spatial order estimation. Non-empty, disjoint intersections* $P_1 = (A_1 \cap A_3) - A_2$, $P_2 = (A_2 \cap A_3) - A_1$, $P_3 = (A_1 \cap A_2) - A_3$, $P_4 = A_1 \cap A_3 \cap A_2$ *shown.*

in front. For instance in Fig. 7.1, we can infer that $1 > 3$ since the mean intensity in P_1, is closer to c_1 than to c_3. A similar comparison of the mean intensity in P_4 with c_2 and c_3, gives $1 > 2$ and $1 > 3$. For the mean-intensity in an intersection to give consistent information about object occlusions, we need the following assumptions:

- The intensity in the regions A_p formed by the objects is close to a constant c_p, and is *different* for objects that occlude each other. This allows us to identify based on mean intensity, the object that an intersection region is part of.
- Objects do not twist between themselves, i.e. if O_i occludes O_j in some region, O_i is *not occluded* by O_j in any region. This is to define a valid order relation for the objects based on their intersection regions.

Then the region covering all the objects, $A = \bigcup_{p=1}^{N} A_p$, can be written down as a disjoint union of $2^N - 1$ regions, where the image intensity is close to a constant in each of those regions. Of these regions, N regions are the visible parts of the objects O_k, with intensity c_k. The rest of the $2^N - N - 1$ regions is where occlusions can possibly occur. The intensities in these regions are close one of the object intensities, c_k, i.e. the intensity of the object in front. So we look at the mean-intensity μ_P in a non-empty intersection region P, and infer that the object say, O_f whose intensity c_f is the closest to μ_P, is in front of the other objects that occur in the intersection.

If P is an intersection of p objects, (WLOG),

$$P = \{\cap_{s=1}^{p} A_s\} - \{\cup_{s=p+1}^{N} A_s\},\ p > 1,$$

we can infer that the object in front, O_f, from

$$f = \min_{1 \le s \le p} (\mu_P - c_s)^2, \tag{7.1}$$

μ_P, the mean image intensity in P, can be linearly expressed in terms of the constants $c_q,\ c_{q,k},\ q \le p$. Thus inspecting the intersection region P gives $f > s, (s = 1, 2, ..f - 1, f + 1, ..p)$.

To illustrate the procedure, for $N = 2$ case, from (3.2), we have:

$$\begin{aligned} I &= c_1\chi_{A_1} + c_2\chi_{A_2} - c_{2,1}\chi_{A_1\cap A_2} + \tilde{c}\chi_{A_1^c\cap A_2^c} \\ &= c_1\chi_{A_1-A_2} + c_2\chi_{A_2-A_1} + (c_1 + c_2 - c_{2,1})\chi_{A_1\cap A_2} + \tilde{c}\chi_{A_1^c\cap A_2^c}. \end{aligned}$$

Thus, if $P = A_1 \cap A_2 \neq \{\phi\}$, then,

$$\mu_P = \frac{\int_P I dx}{\int_P dx} = c_1 + c_2 - c_{2,1} \tag{7.2}$$

To infer the occlusion relation for O_1 and O_2, we notice that if

$$(c_2 - c_{2,1})^2 = (\mu_P - c_1)^2 < (\mu_P - c_2)^2 = (c_1 - c_{2,1})^2,$$

then O_1 occludes O_2 $(1 > 2)$ and vice versa.

7.2. Spatial order. Previously, we deduced the occlusion relation from intersection regions. Now for the above relation to actually give us a unique spatial ordering of the objects, we need the following assumptions:

- For the objects O_i, O_j, O_k, if $i > j$ and $j > k$, then $i > k$ (i.e. *transitivity*). This falls in line with the assumption that the objects do not twist, hence $k \not> i$. This assumption also allows us extend the relation to objects that do not directly intersect.
- each pair of objects can be compared (either directly or through the transitivity assumption). In other words, there are sufficient number of relevant, nonempty intersection regions to uniquely determine the spatial order.

To summarize, after minimizing (6.1), we look at the mean intensities (which depends linearly on the minimizers C_{int}^{min} and C_{obj}^{min}) in the object intersection regions, to define the occlusion relation. When the given image satisfies the assumptions listed above, a unique spatial order for the objects is recovered. In Fig. 7.1, by inspection of P_1 and P_2, $1 > 3$ and $3 > 2$ follow. By transitivity, the spatial order $1 > 3 > 2$ follows.

Note 1: In this work, due to the constant intensity assumption in the regions A_p, we use mean-intensity to test for occlusions. Hence we used the distance measure $D(I_0|_P, I_0|_{A_s}) = (\mu_P - c_s)^2$ in (7.1), to compare the image distribution in the intersection region P, with the distribution in an object region A_s. D can be easily extended to other distance measures to compare general image distributions.

Note 2: The cost of solving the linear system for C_{int}^n is $O(2^{3N})$, *per* gradient descent iteration n of (6.1). After minimization, one can directly project the estimated sequence C_{int}^{min} onto the set $\mathbf{S}$ to infer the spatial order, which has a high complexity $O(2^N N!)$. In the procedure we have used, no additional cost is incurred in determining the spatial order. To see this, given the object regions A_k, $k = 1, 2, .., N$, the best case is when we can look at just 2 object intersections to successively determine e.g. $1 > 2$, $2 > 3$,..,$N - 1 > N$ giving the spatial order, which is $O(N)$. In the worst case, we have to successively inspect, the N object intersection to determine e.g. $1 > s, (s = 2, 3, ..N)$, then a $N - 1$ object intersection to determine $2 > s, (s = 3, 4, ..N)$, and so on. In such a case, the spatial order is given in $O(N^2)$. Also, the cost of converting C_{int}^{min} into mean-intensities is $O(2^{2N})$(since the transformation matrix is triangular). Thus the total cost for the worst-case scenario is

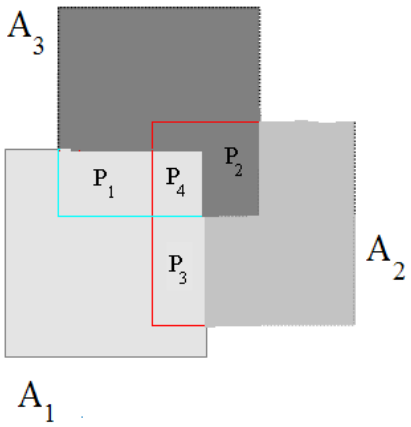

FIG. 8.1. *Selective use of shape. Want shape influence* ***only*** *to Red and Cyan curves (occluded boundaries of* A_2 *and* A_3*).*

$O(N^2 + 2^{2N}) = O(2^{2N})$. However, the above $O(2^{2N})$ cost can be neglected since it has already been accounted for in the $O(2^{3N})$ cost in solving the linear system for C_{int}^n, every iteration n.

8. Selective Shape Term. Since we are dealing with occlusions in multi-object segmentation, prior shape information of the objects is used to fill in missing boundaries in occluded regions. However, just adding a shape term as in (6.2) means that the shape term might influence boundary shapes even in unoccluded regions, where the boundary is unambiguously defined by image intensity. Hence, we introduce our shape term in a selective manner. That is, the shape term is allowed to take effect only for occluded boundaries. From the previous section, we see that the constants C_{int} encode spatial order information, which we use here to impose shape constraints selectively.

To motivate the term, in Fig. 8.1, we want the shape term to *influence only* the red and cyan curves (occluded boundaries of A_2 and A_3). That is, for $P_1 = A_1 \cap A_3 - A_2$, we want to influence only the part of the boundary of P_1 which belongs to the occluded object, i.e the A_3-*boundary*. Similarly, we want to influence only, the A_2-boundary of P_2, the A_2-boundary of P_3, and the A_2,A_3-boundaries of P_4. For P_1, a comparison of μ_{P_1} with c_1 and c_3 would tell us that A_3 is occluded. Then to influence the shape of only the A_3-boundary of P_1, we can restrict the shape term only to the region $A_1 - A_2$. Thus for P_1, we can use a local shape term,

$$\int_{A_3-A_2} (\mu_{P_1} - c_1)^2 \hat{S}(A_1)\, dx + \int_{A_1-A_2} (\mu_{P_1} - c_3)^2 \hat{S}(A_3)\, dx \tag{8.1}$$

Since μ_{P_1} is very close to c_1, the first term is close to zero, and the shape term does not take effect for A_1. For the second term, $(\mu_{P_1} - c_3)^2$ is considerably larger, so the shape term for A_3 is active in the region $A_1 - A_2$, and hence influences only the A_3-boundary of P_1. Similar to the above expression, we can define local shape terms for P_2, P_3, and P_4. Thus we would have a local influence of shape only to the occluded boundaries of A_2 and A_3.

We follow the above idea for the general case. For each intersection region of p objects, $p > 1$, (WLOG)

$$P = \{\cap_{s=1}^{p} A_s\} - \{\cup_{s=p+1}^{N} A_s\},$$

consider the following shape term,

$$\sum_{s=1}^{p} \int_{P_s} (\mu_P - c_s)^2 \hat{S}(A_s)\ dx. \tag{8.2}$$

Here, $P_s = \bigcap_{\substack{t=1 \\ t \neq s}}^{p} A_t - \{\cup_{s=p+1}^{N} A_s\}$. The above shape term localizes use of shape only to boundaries of P that belong to occluded objects. Firstly, the terms $\hat{S}(A_s)$, that constrain the shape of A_s, are weighted by $(\mu_P - c_s)^2$, which is larger for occluded objects, and is minimal for the object that is in front. Secondly, the shape term (8.2) is defined only on P_s, the region that occludes the A_s-boundary of P.

Now, for $N = 2$, we present the modified energy with the local shape term. For the intersection $P = A_1 \cap A_2$ with mean intensity μ, the local shape term defined by (8.2) in level set formulation is

$$\int_{\Omega} H(\phi_2)(\mu - c_1)^2 \hat{S}(\phi_1) + H(\phi_1)(\mu - c_2)^2 \hat{S}(\phi_2) dx$$

Denote $I = c_1 H(\phi_1) + c_2 H(\phi_2) - c_{2,1} H(\phi_1) H(\phi_2) + \tilde{c}(1 - H(\phi_1))(1 - H(\phi_2))$. Since $\mu = c_1 + c_2 - c_{2,1}$ from (7.2), the energy (6.2) with the local shape term becomes:

$$\begin{aligned} &E[\phi_1, \phi_2, c_1, c_2, c_{2,1}, \tilde{c}] = \\ &\int_{\Omega} (I_0 - I)^2 dx + \lambda \Big(\int_{\Omega} |\nabla H(\phi_1) + \int_{\Omega} |\nabla H(\phi_2)| \Big) + \beta \int_{\Omega} \hat{S}(\phi_1) + \hat{S}(\phi_2) dx \\ &\qquad + \tilde{\beta} \int_{\Omega} H(\phi_2)(c_{2,1} - c_2)^2 \hat{S}(\phi_1) + H(\phi_1)(c_{2,1} - c_1)^2 \hat{S}(\phi_2) dx \end{aligned} \tag{8.3}$$

Here, the fourth term is the shape term used to globally influence the shape of the segmented objects to avoid local minima. β and $\tilde{\beta}$ balance the shape terms with $\tilde{\beta} \gg \beta$.

9. Numerical Implementation. In this paper, given the binary image S of a prior shape, we use the symmetric area measure to compare shapes. Hence, in (6.1), the shape term is $\hat{S}(\phi_k) = (H(\phi_k) - S \circ T_k)^2$. T_k are rigid transformations, which have to be determined during minimization. To minimize (6.1), we use a finite difference scheme to solve the resulting Euler Lagrange equations.

We present the numerical implementation for $N = 2$ case, shown in (8.3). Denote $T = [T_1, T_2]$, where $T_k = [\mu_k, \theta_k, \mathbf{t}_k]$, $k = 1, 2$ are rigid transformations with scale μ_k, rotation θ_k and translation $\mathbf{t}_k$. Also, $\Phi = [\phi_1, \phi_2]$ and $C = [c_1, c_2, c_{2,1}, \tilde{c}]$. Rewriting (8.3) using the shape term shown above,

$$\begin{aligned} &E[\Phi, C, T] = \\ &\int_{\Omega} (I - I_0)^2 dx + \lambda \Big(\int_{\Omega} |\nabla H(\phi_1) + \int_{\Omega} |\nabla H(\phi_2)| \Big) + \int_{\Omega} \{\beta + \tilde{\beta} H(\phi_2)(c_{2,1} - c_2)^2)\} \\ &(H(\phi_1) - S \circ T_1)^2 dx + \int_{\Omega} \{\beta + \tilde{\beta} H(\phi_1)(c_{2,1} - c_1)^2\} (H(\phi_2) - S \circ T_2)^2 dx \end{aligned} \tag{9.1}$$

Given (Φ, T), the minimizing constants C of the above energy are easily computed as the solution of a linear system. For an index $k \in \{1, 2\}$, let $\bar{k}$ denote its complement. For $k = 1, 2$, the Euler Lagrange equations for (9.1) are:

$$\delta(\phi_k)\{(I - I_0)(c_{\bar{k}} - c_{2,1}H(\phi_{\bar{k}}) - \tilde{c}(1 - H(\phi_{\bar{k}}))) - \lambda\nabla \cdot \frac{\nabla\phi_k}{|\nabla\phi_k|} +$$

$$\{\beta + \tilde{\beta}H(\phi_{\bar{k}})(c_{2,1} - c_{\bar{k}})^2)\}(H(\phi_k) - S \circ T_k) + \tilde{\beta}(c_{2,1} - c_k)^2(H(\phi_{\bar{k}}) - S \circ T_{\bar{k}})^2\} = 0$$

$$\frac{\partial\phi_k}{\partial\vec{n}} = 0 \quad \text{on} \quad \partial\Omega. \tag{9.2}$$

$$\mu_k \int_\Omega \{\beta + \tilde{\beta}H(\phi_{\bar{k}})(c_{2,1} - c_{\bar{k}})^2)\}(S \circ T_k - H(\phi_k))\nabla S_{T_k x} \cdot R'_{\theta_k} x \; dx = 0, \tag{9.3}$$

$$\int_\Omega \{\beta + \tilde{\beta}H(\phi_{\bar{k}})(c_{2,1} - c_{\bar{k}})^2)\}(S \circ T_k - H(\phi_k))\nabla S_{T_k x} \cdot R_{\theta_k} x \; dx = 0, \tag{9.4}$$

$$\int_\Omega \{\beta + \tilde{\beta}H(\phi_{\bar{k}})(c_{2,1} - c_{\bar{k}})^2)\}(S \circ T_k - H(\phi_k))\nabla S_{T_k x} \; dx = 0 \tag{9.5}$$

Given initial values Φ_0, C_0, and T_0, we use an iterative scheme to minimize (9.1), by sequentially updating Φ, C, and T using gradient descent.

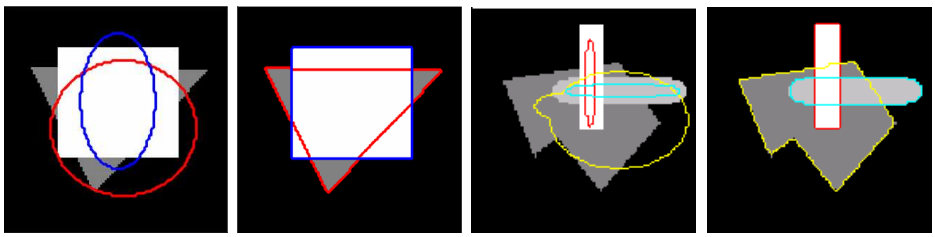

(I) Initialization (II) Result (III) Initialization (IV) Result

FIG. 10.1. *Segmentation of objects with occluded linear boundaries, using* ***only*** *the length term.*

10. Experimental Results. In this section, we present experimental results using (6.1) on synthetic images and a EM (electron microscope) image of erythrocytes, with multiple occluded objects. We demonstrate use of prior shape information in the form of length (Fig.10.1) and explicit shape (Fig.10.3, Fig.10.2) to handle occlusions. Once the mean intensities are obtained for occlusion regions using the minimizing constants C_{int} and C_{obj}, we show in examples (Fig.10.3) how the occlusion relation can be deduced for the objects. Finally in (Fig.10.5 and Fig.10.6), we see how these relationships have been used to impose shape constraints selectively.

10.1. Segmentation with length and explicit shape. In the images in Fig.10.1, we assume that only *linear segments* of objects are occluded. Setting $\beta = 0$ in (6.2), we see that the length term alone can be used to resolve segmentation in occluded regions. Starting with initial level sets $\{\phi_k\}_{k=1}^{N}$ (N$\leq$ max. number of objects expected) shown in (I, III), we minimize (6.2) to obtain segmentation results in (II, IV). The initial level sets have to be overlayed at least partially on the corresponding objects, to avoid local minima. The constants C_{int} and C_{obj} can be arbitrarily initialized.

In the next set of examples in Fig.10.2 and Fig.10.3, we assume that explicit shape information on the objects is available. In Fig.10.2, given an image with occlusions (I), in which the objects can be described by a prior shape (binary image shown on left), we minimize (8.3) using (9.2-9.4) to get the result in (II). The only initial values required here are the initial level sets (shown in I). Using this, a few iterations of the equations (9.3-9.4), are used to get an initial guess for the rigid transformation T_k. Fig.10.3 shows an example for the 3 objects case. Notice that use of prior shape information has resulted in a good segmentation in spite of lack of any intensity information (e.g. Image B).

In Fig.10.4 (I), we see a given EM image of erythrocytes (red blood cells), which are generally known to have a circular surface structure. Naturally, we use a prior shape of a circle in this case, to resolve occlusions. Starting with a initial guess for the active contours in (II), we arrive at result (IV), which is not possible without prior shape information (III).

Shape prior (I) Initialization (II) Result

FIG. 10.2. *Occluded boundaries for 2 objects are detected due to the use of explicit shape.*

10.2. Spatial Order estimation. An immediate application of computing the constants C_{int}, C_{obj} by minimizing (6.1), is to deduce the occlusion relation between the objects. This relation defines a unique object spatial order for images that satisfy the assumptions discussed in Section 7. In the examples shown so far, a unique spatial order exists for Fig. 10.1, Fig. 10.2, and Fig. 10.3 (image A), but does not exist for Fig. 10.3 (image B), and Fig. 10.4.

We demonstrate the procedure described in Section 7 for Fig. 10.3 (image A). The segmented object regions are given by the characteristic functions $\mathrm{H}(\phi_\mathrm{k}) := \mathrm{H_k}$. In Fig. 10.3(II), $\mathrm{H_1}$, $\mathrm{H_2}$, and $\mathrm{H_3}$ are the interiors of the Red, Yellow, and Cyan curves respectively. Let $\bar{\mathrm{H}}_\mathrm{k} := 1 - \mathrm{H_k}$. Now, the object regions $\mathrm{H_k}$, define 4 occlusion regions,

$$\mathrm{P_1} = \mathrm{H_1H_2}\bar{\mathrm{H}}_3, \mathrm{P_2} = \mathrm{H_1}\bar{\mathrm{H}}_2\mathrm{H_3}, \mathrm{P_3} = \bar{\mathrm{H}}_1\mathrm{H_2H_3}, \mathrm{P_4} = \mathrm{H_1H_2H_3}.$$

The computed constants C_{obj}, C_{int} were

$$c_1 = 128.9, c_2 = 191.9, c_3 = 254.3, c_{2,1} = 129, c_{2,2} = 129.1, c_{2,3} = 192, c_{3,1} = 129.1$$

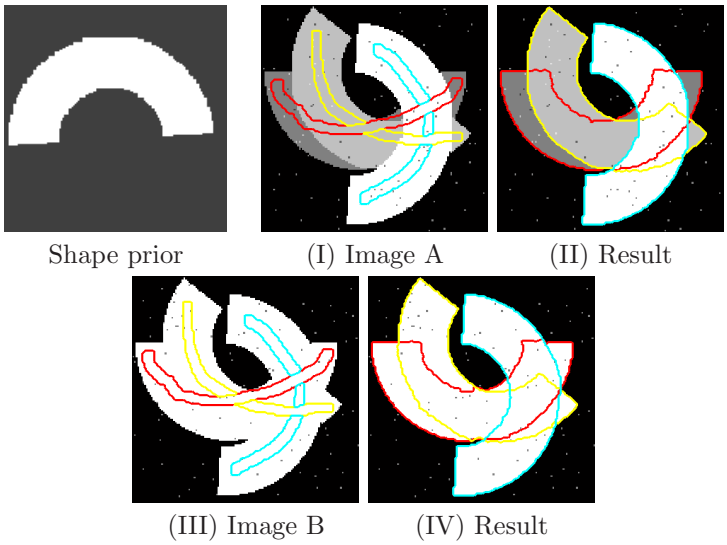

FIG. 10.3. *Segmentation of 3 occluded objects with explicit shape. For the 2 images (A and B), (I and III) shows the input image with the initial guess, and (II and IV) shows the result. Correct result is obtained for Image B despite lack of contrast.*

The following table shows a comparison for these intensities in different occlusion regions. The third column shows the mean intensities μ_k corresponding to the regions P_k, that can be computed from C_{obj}, C_{int} (as shown in the second column).

TABLE 10.1
Comparison of mean intensities in different regions

Occlusion Region	Mean-Intensity,(μ_k)	Values
P_1	$c_1 + c_2 - c_{2,1}$	191.8
P_2	$c_1 - c_{2,2} + c_3$	254.1
P_3	$-c_{2,3} + c_2 + c_3$	254.1
P_4	$c_{3,1}+c_{2,1}+c_{2,2}+c_{2,3}-c_1-c_2-c_3$	254

When we compare the mean intensities μ_k with C_{obj}, we can infer the occlusion relation as follows,

$$|\mu_1 - c_2| < |\mu_1 - c_1| \text{ gives, } 2 > 1, \text{ and}$$
$$|\mu_3 - c_3| < |\mu_3 - c_2| \text{ gives, } 3 > 2.$$

which due to the transitivity assumption gives the unique spatial ordering of the objects as $3 > 2 > 1$, i.e. O_3, O_2, O_1 (with increasing depth).

10.3. Selective use of shape. Finally, we will see examples where we have used the occlusion relation to impose shape constraints selectively. In Fig. 10.5, we see an image of two objects say (W (white) and G (gray)), with W occluding G. In addition, the object in front W has sharp features in the intersection region, which we want the segmentation to preserve. Assuming occluded boundaries to be linear, only the length term is used to resolve occlusions. In (II), we minimized (6.2) with $\beta = 0$.

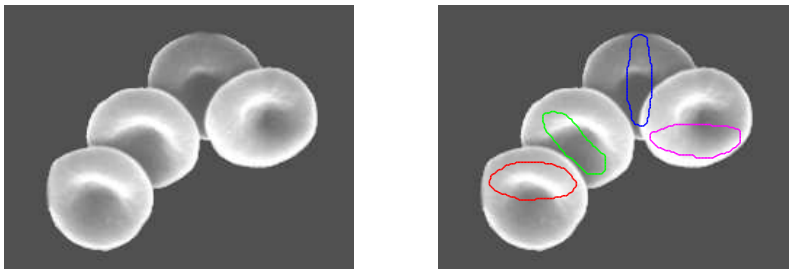

(I) Original Image (II) Initialization

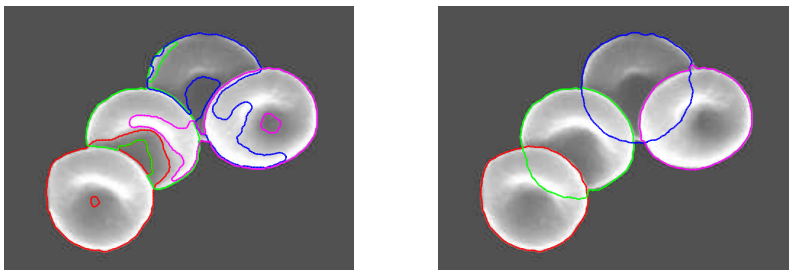

(III) Without shape prior (IV) With a circular shape prior

FIG. 10.4. *Segmentation of erythrocytes in EM image. (I) Input image with circular shaped objects. (II) Initial contours that have to be placed close to the objects (III) Incorrect result without use of shape due to occlusions (IV) Correct result with use of a circular shape prior.*

.

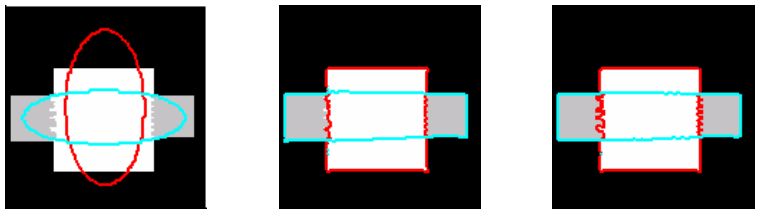

I II III

FIG. 10.5. *Selective use of length only for occluded boundaries. (I) Initialization (II) Without selective use of length, the sharp features in the white object are lost (III) With a selective length term, the features of the white object are recovered.*

The resulting segmentation has correctly filled in the missing linear boundaries for G, but has not segmented W correctly, since the use of length term evenly, for both the objects has resulted in the loss of sharp features in W. When we use a selective length term as in (8.3) with $\hat{S}(\phi_k) = |\nabla H(\phi_k)|$ and setting the parameters $\tilde{\beta} = 0, \lambda \ll \beta$, the required boundaries are computed as needed (III). Notice that the length term is effected only for the object that is occluded G, hence preserving the features of W.

A similar example is presented in Fig. 10.6, with use of explicit shape. Here (I) shows two *square* shaped objects W & G with W occluding G, and each with one of their corners chipped off. We want our segmentation to be able to complete the missing boundary for G in the occlusion region, and also be able to preserve edges that are not occluded. (II) shows the result when a shape term is not used; the length term

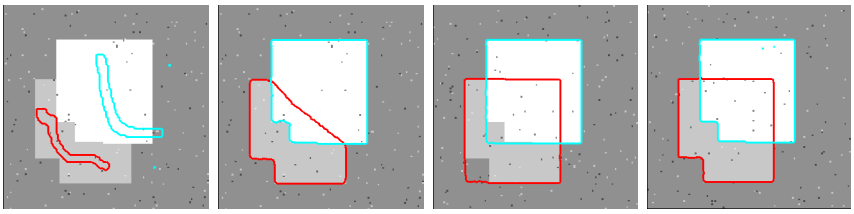

FIG. 10.6. *Selective use of Shape (I) Initialization (II) Without shape. Only the length term is active. (III) Without selective shape, the chipped corners are not segmented due the influence from the shape term. (IV) With selective shape, the corners are detected and the occluded boundary of the gray object is also recovered.*

completes the occluded part of G linearly. (III) shows the result with a uniform shape term as in (8.3). Notice that the corners of both W & G are not segmented properly, due to the influence of the shape term even to non occluded regions. Finally, we get the correct segmentation in (IV), using a selective shape term as in (9.1). Firstly, use of the shape term has filled the missing boundary of G that has been occluded. Secondly, the shape term is applied only to the occluded object G. Hence the corner of W is recovered. Thirdly, the shape term applied to G is effected only within the object W, thus localizing the effect of shape on G. Hence the corner of G is also recovered.

11. Comparisons. In Section 5, we showed that the NMS minimization (2.3)

$$\min_{k\in\{1,2,...N!\}} \min_{\mathbf{A},C_{obj}} \tilde{E}_{Q^k}$$

is equivalent to our constrained minimization (4.1)

$$\min_{\mathbf{A},C_{obj},C_{int}\in\{S^1,S^2,...,S^{N!}\}} E.$$

In the previous sections, we dealt with the implementation details and experiments for the unconstrained minimization (4.2)

$$\min_{\mathbf{A},C_{obj},C_{int}} E.$$

Now, we will provide a detailed comparison of computational complexities of (2.3) with (4.1). Then for a typical example with varying noise levels, we compare the solutions obtained by the energy (4.1) with its unconstrained version (4.2) that we use for our experiments.

Here, for the implementation of (2.3) and (4.1), we used an iterative gradient descent scheme as shown for (4.2). To impose the constraint on C_{int} for (4.1), during each iteration n, we project the sequence C_{int}^n onto $\mathbf{S}$ when such a projection is uniquely defined. To avoid local minima issues, if such a projection is not uniquely defined, we simply retain the value of C_{int}^n for the next iteration.

11.1. Complexity comparisons of (4.1) with NMS energies. The key difference between the (NMS) energy and our formulation is the estimation of the spatial order of the objects. In our model, firstly we note that there is a one-one correspondence between the spatial orders $\mathbf{Q} = \{Q^1, Q^2, ..., Q^{N!}\}$ and the sequences

$\mathbf{S} = \{S^1, S^2, ..., S^{N!}\}$. Thus in our constrained formulation (4.1), the spatial order is given by the estimated value of C_{int}. We show an example to illustrate the spatial order estimation in our case. In Fig.11.1, (I) is an image with 3 objects with a "half moon" shape. The initial contours are shown overlay-ed on the objects. (II) shows the segmented contours using gradient descent of (4.1) which converged in about 1000 iterations.

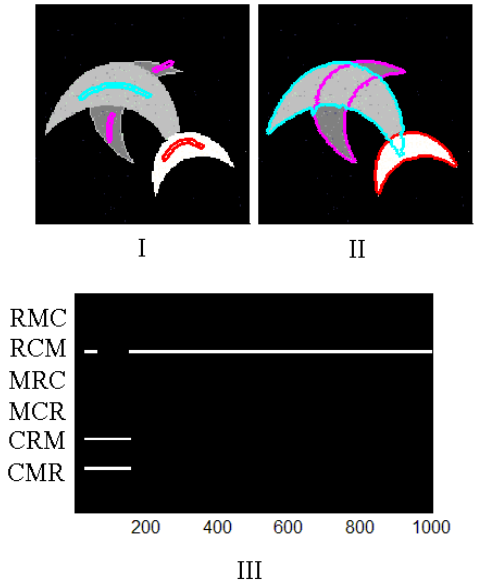

FIG. 11.1. *Spatial order estimation through variable C_{int}. (I) Image with initial guess (II) Segmented contours (III) Plot of possible Spatial orders (Y axis) against iteration (X axis) (e.g. between iterations $100 - 200$, CRM and CMR are the possible spatial orders).*

In the graph (III) (*iteration vs spatial order*), we see the spatial order corresponding to the estimated C^n_{int}. The spatial order (Y axis) between the objects (labelled by colors (Red(R), Magenta(M), Cyan(C))) is indicated by e.g. RMC denotes the order R > M > C. The first few iterations when the evolving object regions have not yet intersected, C^n_{int} is unknown. Then, until about 200 iterations, the projection of C^n_{int} to the spatial order set $\{S^1, S^2, ..., S^{N!}\}$ is not unique. Finally after 200 iterations, when a sufficient number of intersection regions between the evolving objects are non empty, the projection of C^n_{int} to $\mathbf{S}$ is unique and hence defines the spatial order.

In the (NMS) approach (2.3), there are $N!$ energies $\tilde{E}_{Q^k}(C_{obj}, \mathbf{A}), k = 1, 2.., N!$ one minimizes. The spatial order is then given by the smallest of the above energy-minima. Even in case of a good initial guess for the object boundaries, one would have to go through the $N!$ minimizations. Thus, even though the search space is the same for both (NMS) and our energies, unlike the (NMS) approach, our model determines the spatial order by gradient descent of C_{int}. Since the spatial order is integrated within a *single energy*, our model involves N level set minimizations in contrast to $N.N!$ level set minimizations in the (NMS) model. The level set evolution is the *main cost* in both cases, which is $O(M^2)$ for grid size M^2. In fact, one gradient descent

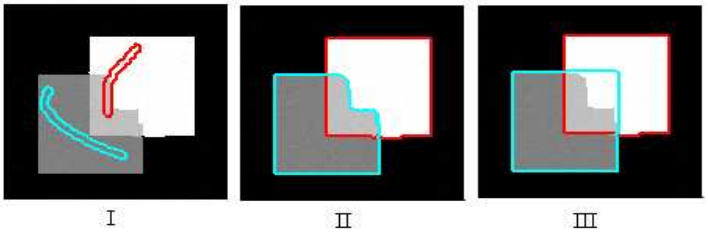

FIG. 11.2. *Solutions computed using (4.1) and (6.1) for spectral noise images. (I) Image of 2 objects (white and dark gray) with noise induced edges (due to the light gray region) (II) Incorrect Result using (4.1) (segmentation of cyan curve influenced by image term). (III) Correct Result using (4.1) (segmentation of cyan curve influenced only by shape term).*

iteration in the (NMS) model has a high complexity $O(N!.(N.M^2))$.

In our case, one iteration is a much lesser $O(N.M^2 + 2^{3N} + 2^N N!) = O(N.M^2 + 2^N N!)$. As before, the N level set minimizations is $O(N.M^2)$, solving for the linear system for the constants C_{int} is $O(2^{3N})$, and projecting C_{int} onto the $N!$ constraint set $\mathbf{S} = \{S^1, S^2, ..., S^{N!}\}$ is $O(2^N N!)$. If instead of directly projecting C_{int} onto $\mathbf{S}$, the procedure detailed in Section 7 is used, the cost of computing the spatial order from C_{int} is only $O(2^{2N})$. In this case, our complexity for one iteration becomes $O(N.M^2 + 2^{3N})$.

Note: Our experiments indicate that the energy convergence rate of gradient descent is the *same* for (4.1), and for *one* of the $N!$ (NMS) energies (i.e the energy corresponding to the object spatial order). This observation which is part of ongoing work will be reported in another publication.

11.2. Comparison of (4.1) and its unconstrained version (4.2). For our experiments section, we used the energy (4.2), $E[\mathbf{A}, C_{obj}, C_{int}]$, which is the unconstrained version of (4.1), i.e. $E[\mathbf{A}, C_{obj}, C_{int} \in \mathbf{S}]$. For images corrupted with white noise, our experiments indicate that the minimizers computed using the above energies are very close. This is not true in general for non-white (*spectral*) noise images, since (4.2) due to the additional constants C_{int} intrinsically allows the intensities in the intersection regions to be different from the object intensities. Thus the resulting segmentation of occluded objects could be influenced by edges introduced by noise. For instance, in Fig. 11.2(I) shows an image with spectral noise (in the light gray region) that corrupts the intersection of the 2 square objects (white and dark gray regions). (II) shows the incorrect segmentation obtained by the energy (4.2). To make the intersection region close to constant intensity, the image term competes with the shape term and has influenced the shape of the cyan curve (occluded object). Thus one would have to tune the shape parameter β in (4.2) to get to a minimizer close to that of (4.1) (shown in (III)). Whereas the result computed using (4.1) is robust to such types of noise, because once the spatial order is determined (i.e. projection of C_{int} onto $\mathbf{S}$ is unique), occluded boundaries are driven *only* by the shape term. Hence tuning of β is not required in this case.

Now we illustrate 2 examples in Figure.12.1 for $N = 2, 3$ to compare solutions of the above models for varying white-noise levels. The results for both models were obtained for the same values of the shape parameter β chosen nominally without any careful tuning. In both examples, we see *identical* segmentation results using

(4.2)(A) and (4.1)(B) for images corrupted with increasing levels of white noise. For $N = 2, 3$, the plot shown is the relative-error $\xi(\%)$ (Y-axis) with respect to noise level (X-axis). Here $\xi = \text{mean}(\frac{|A_i - B_i|}{|B_i|}, i = 1, 2, ..N)$, where A_i are the segmented regions using (4.2) and B_i are the corresponding segmented regions using (4.1). Likewise, the errors obtained for the object intensities were very low and the estimated spatial orders were identical for both models. The low errors observed above indicate that for white-noise images, the minimizers are not dependent on the constraint on C_{int}.

12. Conclusion. We have presented a variational energy based framework (4.1) to segment multiple occluded objects using prior shape information of the objects. We note that the spatial order between the objects are encoded within the constants C_{int} which we estimate as part of the minimization process. Our model as we demonstrated is computationally less expensive than the NMS approach (2.3) which formulates segmentation energies for each spatial order. Secondly we showed how the estimated constants C_{int} and C_{obj} can be used to impose shape priors selectively, just to occluded boundaries. Also in our experiments, we have approximated the energy (4.1) by its unconstrained version (4.2) and the results for the above energies are observed to be identical for white noise images. As future work, we want to prove the above observation and provide error estimates for spectral noise images. Secondly, in our experiments the initial contours have to be placed near the objects to avoid local minima. This might not be practicable for applications with a large number of objects. Hence another direction is to automate the contour initialization procedure to extend the EMI example (Fig. 10.4) to applications such as automatic counting of blood cells. Finally, we have used one level set per object irrespective of the occlusion scene. A better way would be to use an optimal number of level set functions depending on the occlusion scene. For instance, when N objects occlude each other in all possible regions, we definitely need N level sets, whereas when no occlusions occur, one can work with $\log_2 N$ level sets (e.g. multiphase CV).

REFERENCES

[1] G. Bertrand and G. Malandain. A new topological segmentation of discrete surfaces. In *European Conference on Computer Vision*, pages 710–714, 1992.

[2] A. Blake and A. Zisserman. *Visual reconstruction*. MIT press, 1987.

[3] V. Caselles, F. Catte, T. Coll, and F. Dibos. A geometric model for active contours. *Nümerische Mathematik*, 66:1–31, 1993.

[4] V. Caselles, R. Kimmel, and G. Sapiro. Geodesic active contours. In *ICCV*, pages 694–699, 1995.

[5] T. Chan and W. Zhu. Level set based shape prior segmentation. In *Proc. CVPR'05*, pages 20–26, 2005.

[6] T.F. Chan and L.A Vese. Active contours without edges. *IEEE Trans. Image Processing*, 10(2):266–277, 2001.

[7] Y. Chen, S. Thiruvenkadam, et al. On the incorporation of shape priors into geometric active contours. In *IEEE Workshop on Variational and Level set Methods*, pages 145–152, 2001.

[8] Yunmei Chen, Hemant Tagare, et al. Using prior shapes in geometric active contours in a variational framework. *IJCV*, 50(3):315–328, 2002.

[9] David L. Chopp. Computing minimal surfaces via level set curvature flow. *Journal of Computational Physics*, 106:77–91, 1993.

[10] L.D. Cohen. On active contour models and balloons. *CVGIP: Image Understanding*, 53:211–218, 1991.

[11] Timothy Cootes, Christopher Taylor, David Cooper, and Jim Graham. Active shape models-their training and application. *CVIU*, 61(1):38–59, 1995.

[12] D. Cremers, N. Sochen, and C. Schnörr. Towards recognition-based variational segmentation

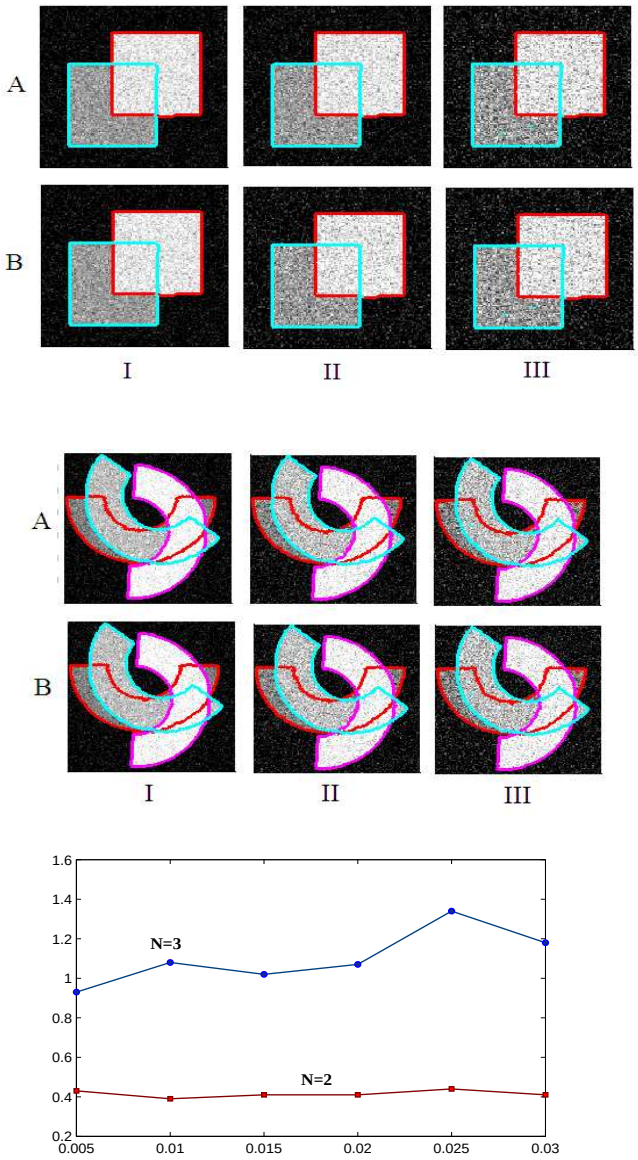

FIG. 12.1. *Comparison of solutions computed using (4.2)(row A) and (4.1)(row B) for noise levels (I) .01 (II) .02 (III) .03. The plots for N=2,3 shows relative-error ξ(%)(Y axis) with respect to noise level (X axis).*

using shape priors and dynamic labeling. In *Proceedings of International Conference on Scale Space Theories in Computer Vision*, 2003.

[13] H. Delingette and J. Montagnat. New algorithms for controlling active contours shape and topology. In *European Conference on Computer Vision*, pages 381–395, 2000.

[14] A. Dervieux and F. Thomasset. A finite element method for the simulation of Rayleigh-Taylor instability. *Lecture Notes in Mathematics*, 771:145–159, 1979.

[15] A. Dervieux and F. Thomasset. Multifluid incompressible flows by a finite element method. In W. Reynolds and R.W. MacCormack, editors, *Seventh International Conference on*

Numerical Methods in Fluid Dynamics, volume 141 of *Lecture Notes in Physics*, pages 158–163, June 1980.

[16] S. Esedoglu and R. March. Segmentation with depth but without detecting junctions. *J. Mathematical Imaging and Vision*, 18(1):7–15, 2003.

[17] P. Fua and Y.G. Leclerc. Model driven edge detection. *Machine Vision and Application*, 3:45–56, 1990.

[18] U. Grenander, Y. Chow, and D. Keenan. *HANDS: A Pattern Theoretic Study of Biological Shapes*. Springer-Verlag, 1990.

[19] M. Kass, A. Witkin, and D. Terzopoulos. Snakes: Active contour models. In *First International Conference on Computer Vision*, pages 259–268, London, June 1987.

[20] S. Kichenassamy, A. Kumar, P. Olver, A. Tannenbaum, and A. Yezzi. Gradient flows and geometric active contour models. In *ICCV*, pages 810–815, 1995.

[21] S. Kichenassamy, A. Kumar, P. Olver, A. Tannenbaum, and A. Yezzi. Conformal curvature flows: from phase transitions to active vision. *Archive for Rational Mechanics and Analysis*, 134:275–301, 1996.

[22] M. Leventon, W. L. Grimson, and O. Faugeras. Statistical shape influence in geodesic active contours. In *CVPR*, volume 1, pages 316–323, 2000.

[23] R. Malladi, J.A. Sethian, and B.C. Vemuri. A topology independent shape modeling scheme. *SPIE*, 2031:246, 1993.

[24] T. McInerney and D. Terzopoulos. Topologically adaptable snakes. In *International Conference on Computer Vision*, pages 840–845, Los Alamitos, California, June 1995.

[25] Rousson Mikaël, Paragios Nikos, and Deriche Rachid. Active shape models from a level set perspective. Technical Report 4984, INRIA, October 2003.

[26] D. Mumford and J. Shah. Boundary detection by minimizing functionals. pages 22–26, 1985.

[27] D. Mumford and J. Shah. Optimal approximations by piecewise smooth functions and associated variational problems. *Comm. on Pure and App. Math.*, 42:577–684, 1989.

[28] M. Nitzberg and D. Mumford. The 2.1-d sketch. In *ICCV*, 1990.

[29] M. Nitzberg, D. Mumford, and T. Shiota. Filtering, segmentation and depth. *Lecture Notes in Computer Science*, 662, 1993.

[30] S. Osher and J. Sethian. Fronts propagating with curvature dependent speed: algorithms based on the Hamilton–Jacobi formulation. *J. of Comp. Phy.*, 79:12–49, 1988.

[31] Nikos Paragios and Rachid Deriche. Coupled geodesic active regions for image segmentation : a level set approach. volume II, pages 224–240, June 2000.

[32] T. Riklin-Raviv, N. Kiryati, and N. Sochen. Unlevel-sets: Geometry and prior-based segmentation. In *ECCV'04*, volume LNCS 2034, pages 50–61, 2004.

[33] A. Tsai, A. Yezzi, et al. Model-based curve evolution technique for image segmentation. In *In Proc. CVPR'01*, volume 1, pages 463–468, December 2001.

[34] A. Tsai, A. Yezzi, and A.S. Willsky. Curve evolution implementation of the mumford-shah functional for image segmentation, denoising, interpolation, and magnification. *IEEE Trans. on IP*, 10:1169–1186, 2001.

[35] L. Vese and T. Chan. Multiphase level set framework for image segmentation using the mumford and shah model. *IJCV*, 50(3):271–293, 2002.

[36] T. Chan W. Zhu and S. Esedoglu. Segmentation with depth: A level set approach. *UCLA CAM report*, (04-49), 2004.

[37] A. Yezzi, A. Tsai, and A. Willsky. A statistical approach to snakes for bimodal and trimodal imagery. volume II, pages 898–903, September 1999.